PERGAMON

International Journal of Heat and Mass Transfer 43 (2000) 3551–3566

International Journal of HEAT and MASS TRANSFER

www.elsevier.com/locate/ijhmt

Mechanisms for the heat transfer enhancement in zero-mean oscillatory flows in short channels

P. Li*, K.T. Yang

Department of Aerospace and Mechanical Engineering, University of Notre Dame, Notre Dame, IN 46556, USA

Received 21 May 1999; received in revised form 10 December 1999

Abstract

The fluid mechanics and heat transfer of zero-mean oscillatory flows at low frequencies and large amplitudes in essentially two-dimensional short channels are studied numerically. The results show that intracycle oscillations do also occur, and that such oscillations are different from those for long ducts. In the case of sudden pressure changes as the flow reverses at the ends, the intracycle oscillations are found to occur in the acceleration phase of the oscillatory cycle and are responsible for the heat transfer enhancement. These results compare favorably with previously obtained experimental data.

1. Introduction

It is now well recognized that studies in the enhancement of convective heat transfer must be pursued on a long-term basis to insure the availability of adequate and feasible techniques demanded by applications. One broad area of heat-transfer schemes which has received much attention in recent years is the use of oscillatory flows to enhance heat transfer. A general review has been recently given by Cooper et al. [1]. Since then, additional experimental results dealing with zero-mean oscillatory flows have been reported by Cooper et al. [2], Zhao and Cheng [3], Qiu and Simon [4], Walsh et al. [5], and Liao et al. [6], which all show significantly enhanced heat transfer in ducts and enclosures. It is apparent that the full potential of the zero-mean oscillatory flow in heat-transfer applications cannot be properly exploited without an understanding of the exact physical mechanisms involved. Unfortunately, even though such mechanisms have been proposed in the recent literature [7–10], they are not all in agreement.

One important issue pertinent to the mechanism of heat transfer enhancement in zero-mean oscillatory flow is laminar-turbulent transition. Whether or not the transition indeed occurred in the experiments mentioned above is the focus of disagreement. Another is whether there are other mechanisms which could also lead to enhanced heat transfer. In the more recent experiments of Cooper et al. [2], heat transfer enhancement has also been observed in relatively short channels at low frequencies and large amplitudes. Flow instabilities require time to evolve and they are difficult to occur in short channels, since the flow must stop before it reverses. It is intuitively clear that for short channels, the boundary conditions at the channel ends must have an important effect. The purpose of this study is to determine these end effects and see if these effects would closely explain the enhancement data of [2] for such short channels.

* Corresponding author. Present address: Vickers Incorporated, Jackson, Mississippi.

0017-9310/00/$ - see front matter
PII: S0017-9310(99)00390-7

Nomenclature

D	channel height, m
g	gravitational acceleration, m/s^2
h	coefficient of heat transfer, W/m^2 K
k	thermal conductivity, W/m K
L	channel length, m
l	heater length, m
Nu	Nusselt number
Pr	Prandtl number
p	dimensionless pressure
q_w	wall heat flux, W/m^2
Re	reference Reynolds number
Re_ω	oscillatory-flow Reynolds number
Ri	Richardson number
T	dimensionless temperature above ambient
T_c	reference temperature, °C
T_s	heater surface temperature, °C
t	dimensionless time
U	velocity, m/s
U_m	average velocity, m/s
u	dimensionless x-direction velocity
u_m	dimensionless average velocity
$u_{max\text{-}m}$	maximum cross-sectional mean velocity in cycle, m/s
$u_{max\text{-}y}(y)$	maximum inlet velocity profile in cycle, m/s
$u_{mea\text{-}c}$	measured maximum velocity at centerline in cycle, m/s
v	dimensionless y-directional velocity
W	depth of channel, m
w	dimensionless z-directional velocity

Greek symbols

α	Womersley number
β	transition number
β_c	coefficient of volumetric expansion, °C^{-1}
δ_s	Stokes layer thickness, m
Δ_x	tidal displacement, m
ν	kinematic viscosity, m^2/s
ρ	density, kg/m^3
ω	circular frequency, rad/s

2. Parameters and physical discussions

For zero-mean oscillatory flow in short channels, pertinent characteristic lengths are obviously the channel length L and height D. However, an additional important third characteristic length is the tidal displacement, Δ_x, defined as the maximum cross-stream averaged distance a fluid particle would move during one-half of an oscillating cycle. It is easily shown that in simple harmonic oscillatory flows, the mean cross-sectional velocity is related to the tidal displacement by

$$u_{max\text{-}m} = \frac{\Delta_x \omega}{2} \tag{1}$$

where ω is the imposed oscillatory circular frequency in rad/s. It is clear that Δ_x is synonymous with the amplitude of the imposed oscillations when the fluid is incompressible. It is intuitively clear that any zero-mean oscillatory flow must necessarily depend on its frequency and tidal displacement (amplitude), along with other geometrical parameters and physical properties. This is evidently also true for the corresponding heat transfer phenomena. Under the condition of incompressible fluids and constant properties inherent in all experimental and theoretical studies now available, a simple dimensional analysis suggests that in addition to various geometrical ratios, there are two independent dimensionless parameters that are related to the frequency and tidal displacement of a zero-mean oscillatory flow. These are the Womersley number α and the transition number β defined, respectively, by [2,7]

$$\alpha = (D/2)\sqrt{\omega/\nu} \qquad \beta = \Delta_x\sqrt{\omega/\nu} \tag{2}$$

where ν is the kinematic viscosity of the fluid. In realizing that the quantity $\sqrt{\nu/\omega}$ is the well-known Stokes-layer thickness due to pure oscillations, it can be seen that the Womersley number α is the ratio of the geometrical half height to the Stokes-layer thickness, and represents a frequency parameter. On the other hand, the transition number β, which has often been used in the oscillatory-flow literature as an indicator for the laminar-turbulent transition, represents the ratio of the tidal displacement to the Stokes-layer thickness [1].

Many researchers have addressed the issue of laminar–turbulent transition in zero-mean oscillatory flows, since one prevailing opinion is that the corresponding heat transfer enhancement is due to this transition. However, a wide range of the transition number β has been reported, even for similar geometries. For flows of liquids in pipes and channels with $\alpha > 3$, a transitional β (independent of α) in the range of 500–550 has been given by a number of investigators [11–13]. On the other hand, Merkli and Thomann [14] observed transition at $\beta \sim 280$ for flow in a pipe with air as the working fluid. It is, however, significant to note that in all these studies, the typical length to diameter or channel height is about 200.

Cooper et al. [2] noted that favorable pressure gradi-

ents, with respect to time, are shown to stabilize the flow while adverse pressure gradients are shown to sustain velocity fluctuations. Unfortunately, several inconsistencies in this experimental data have recently been discovered and tend to cast some doubts on the results presented. Same phenomena have also been observed by Zhao and Cheng [8] and Qiu and Simon [4] for zero-mean oscillatory flows in circular pipes. A correlation equation in terms of α and the dimensionless oscillation amplitude of fluid for the prediction of the onset of turbulence is obtained by Zhao and Cheng [8]. It is somewhat similar to what was suggested by Kurzweg et al. [15]. However, it seems to be odd that the laminar-turbulent transition could be represented by a single curve with no apparent transition zone. The first doubt about the validity of the laminar–turbulent transition mechanism was expressed in the experimental study of [2], in which the intracycle longitudinal velocity components along the channel were measured by hotwire anemometers. Huang et al. [9] simulated Cooper's experiments numerically, trying to verify the theory of laminar high-order intracycle harmonics. Although his results showed good agreement with the experiments, his work is not complete, since he neglected one of the advection terms in the momentum equation which are only valid when the vertical velocities dominate. So the high-order harmonics theory of complex laminar flow is still to be verified.

Another convenient dimensionless parameter, which is not independent of the Womersley and transition numbers, but plays essentially the same role as the Reynolds number in steady flows, is the oscillatory-flow Reynolds number, which unfortunately carries different definitions by different researchers. For the present purpose, the following definition is adopted:

$$Re_\omega = u_{\text{max-m}} D/\nu = \left(\frac{1}{2}\omega\Delta_x\right) D/\nu = \alpha\beta \tag{3}$$

However, it should be noted that this particular relation with α and β is only valid when the oscillatory flow is a simple harmonic motion. Here, it would be of significance to determine the effects of the parameters α, β, and Re_ω for a given geometry on the fluid mechanics and also on the corresponding heat transfer characteristics. For the present problem, a Nusselt number Nu can be defined as

$$Nu = hl/k \tag{4}$$

where h is the coefficient of heat transfer, l is a characteristic length of the heater, and k is the thermal conductivity of the fluid. Here h is taken to be the spatially and temporally averaged coefficient of heat transfer, similar to those utilized by Cooper et al. [2] and Liao et al. [6]. Also for heat transfer, the fluid Prandtl number Pr is yet another parameter, but is taken to be a constant in the present study for air [2]. Also, consideration needs to be given to the effect of buoyancy for the case of a horizontal channel, which may not be negligible as there is a short period of time in which the imposed velocity is close to zero when the flow reverses. This effect is normally given in terms of a Richardson number Ri, to be defined later.

The critical issue in zero-mean oscillatory flows and the associated heat transfer problem is in the determination of whether in the Re_ω, α, β ranges which have been studied so far in the literature, the flows are actually turbulent, as claimed by several of the investigations, or rather, are in reality still in the transition region, as claimed by others. In the latter case, it is also significant to be able to determine the specific stage or stages of transition of the oscillatory flows. The significance of this determination lies in the fact that by knowing the stages in the transition process of the flows, it becomes possible to further exploit the zero-mean oscillatory flows for even higher degrees of heat transfer enhancement. Thus, one of the primary objectives of the present study is to critically examine the current literature on this subject and also carry out additional studies to attempt to resolve this controversy so that the field can move onward for further meaningful studies.

3. Formulation of numerical model

Since one of our primary objectives is to attempt to closely simulate the short-channel data of [2] and then to discover the mechanism for the enhanced heat transfer observed in their experiments, it is important to use a channel geometry conforming to that in the experiments. A schematic of this nearly two-dimensional channel with a length L of 47 cm is shown in Fig. 1. It is clear that the experimental channel is necessarily three-dimensional. However, the width of the channel (15.24 cm) is large as compared to the channel height which is allowed to vary from almost 0 to 7.595 cm. In addition to the channel height D, another characteristic length, used to determine the heat transfer from the heater is the heater length l, which is known to be 6.35 cm. The formulation in the present study is based on the standard equations of continuity, momentum, and energy under the conditions of three-dimensionality, incompressible fluid, negligible dissipation and pressure work, constant fluid properties, and the Boussinesq approximation, along with appropriate boundary conditions, which require serious consideration because of the emphasis on short channels here. The scalings for length, time, velocity, pressure, and temperature are D, $D/u_{\text{max-m}}$, $u_{\text{max-m}}$, $\rho u^2_{\text{max-m}}$ and $T_c = q_w D/k$, respect-

ively. As a result, the governing equations can be written as follows:

Continuity

$$\frac{\partial u}{\partial x}+\frac{\partial v}{\partial y}+\frac{\partial w}{\partial z}=0 \tag{5}$$

Momentum

$$\begin{aligned}&\frac{\partial u}{\partial t}+\frac{\partial(u^2)}{\partial x}+\frac{\partial(uv)}{\partial y}+\frac{\partial(uw)}{\partial z}\\&\quad=-\frac{1}{\rho}\frac{\partial p}{\partial x}+\frac{\partial}{\partial x}\left[\frac{2}{Re}\left(\frac{\partial u}{\partial x}\right)\right]\\&\quad+\frac{\partial}{\partial y}\left[\frac{1}{Re}\left(\frac{\partial u}{\partial y}+\frac{\partial v}{\partial x}\right)\right]\\&\quad+\frac{\partial}{\partial z}\left[\frac{1}{Re}\left(\frac{\partial u}{\partial z}+\frac{\partial w}{\partial x}\right)\right]\end{aligned} \tag{6}$$

$$\begin{aligned}&\frac{\partial v}{\partial t}+\frac{\partial(uv)}{\partial x}+\frac{\partial(v^2)}{\partial y}+\frac{\partial(vw)}{\partial z}\\&\quad=-\frac{1}{\rho}\frac{\partial p}{\partial y}+\frac{\partial}{\partial y}\left[\frac{2}{Re}\left(\frac{\partial v}{\partial y}\right)\right]\\&\quad+\frac{\partial}{\partial x}\left[\frac{1}{Re}\left(\frac{\partial u}{\partial y}+\frac{\partial v}{\partial x}\right)\right]\\&\quad+\frac{\partial}{\partial z}\left[\frac{1}{Re}\left(\frac{\partial v}{\partial z}+\frac{\partial w}{\partial y}\right)\right]+RiT\end{aligned} \tag{7}$$

$$\begin{aligned}&\frac{\partial w}{\partial t}+\frac{\partial(wu)}{\partial x}+\frac{\partial(wv)}{\partial y}+\frac{\partial(w^2)}{\partial z}\\&\quad=-\frac{1}{\rho}\frac{\partial p}{\partial z}+\frac{\partial}{\partial z}\left[\frac{2}{Re}\left(\frac{\partial w}{\partial z}\right)\right]\\&\quad+\frac{\partial}{\partial x}\left[\frac{1}{Re}\left(\frac{\partial u}{\partial z}+\frac{\partial w}{\partial x}\right)\right]\\&\quad+\frac{\partial}{\partial y}\left[\frac{1}{Re}\left(\frac{\partial v}{\partial z}+\frac{\partial w}{\partial y}\right)\right]\end{aligned} \tag{8}$$

Energy

$$\begin{aligned}&\frac{\partial T}{\partial t}+\frac{\partial(uT)}{\partial x}+\frac{\partial(vT)}{\partial y}+\frac{\partial(wT)}{\partial z}\\&\quad=\frac{\partial}{\partial x}\left[\frac{1}{Re\,Pr}\left(\frac{\partial T}{\partial x}\right)\right]+\frac{\partial}{\partial y}\left[\frac{1}{Re\,Pr}\left(\frac{\partial T}{\partial y}\right)\right]\\&\quad+\frac{\partial}{\partial z}\left[\frac{1}{Re\,Pr}\left(\frac{\partial T}{\partial z}\right)\right]\end{aligned} \tag{9}$$

where the reference Reynolds and Richardson numbers, Re and Ri, are given by

$$Re=u_{\text{max-m}}D/\nu \qquad Ri=\frac{\beta_c g T_c D}{u^2_{\text{max-m}}} \tag{10}$$

respectively. The dimensionless p and T refer to pressures and temperatures above the ambient, respectively. The coordinate origin is set at the left-front corner in Fig. 1.

While in numerical study alone, boundary conditions can be arbitrarily prescribed, this is, however, not the case in the present study, where the results are to be compared with their test counterparts. Consequently, the boundary conditions must adhere as closely as possible to what happened in the experiments. This is particularly the situation in this study where the boundary conditions are expected to have significant effects on the results because of the short channels. Details of the experimental test section and the oscillatory-flow driver have already been given in [2] and hence will not be repeated here. However, it is important to mention that upon flow reversals, the upstream intake-port door suddenly closes, while the downstream exhaust-port door suddenly opens, controlled electronically by a microprocessor. This experimental scenario can best be approximated by a sudden pressure change to ambient at the exhaust port when the imposed flow reversals. The thermal boundary conditions at the channel ends are simply that the temperature is that of the ambient for flow going into the

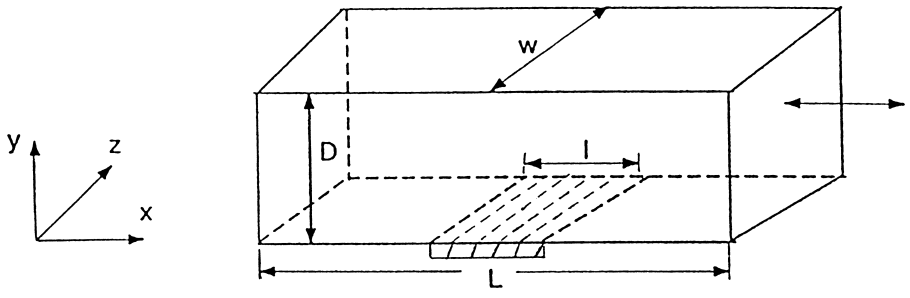

Fig. 1. Channel geometry.

channel and no-flux conditions prevail when the flow leaves the channel. Adiabatic conditions are imposed on all the bounding walls except the region of the heater. A constant heat flux is imposed at the lower surface of the heater. After the system reaches equilibrium, the surface temperature of heater fluctuates periodically, while the amount of heat produced by the heater during each cycle is equal to that carried away by the flow during the same period of time. This equilibrium condition has to be numerically determined first. The unique design of the heater is such that the surface temperature fluctuations were on the order of the noise of the data-acquisition system. Also the time constant of the heater surface is nearly an order of magnitude greater than that of the flow [2]. Consequently, the surface temperatures are essentially constant within the experimental measurement error and this condition is utilized in the simulation studies. Finally, we are not interested in the start-up phenomenon of the zero-mean oscillatory flow, and thus only cyclic long-time solution is sought. This condition is well satisfied by the experimental data. To summarize then, the overall boundary conditions may be stated as (Fig. 1):

(a) When the flow is from the left to right,

$$x = 0 \text{ (left inlet)} \quad u = u_{\text{max-y}}(y)\sin(\omega t),$$

$$v = w = T = 0$$

$$x = L/D \text{ (right outlet)}$$

$$p = \frac{\partial u}{\partial x} = \frac{\partial v}{\partial x} = \frac{\partial w}{\partial x} = \frac{\partial T}{\partial x} = 0$$

$$y = 0, 1 \quad u = v = w = 0, \quad \frac{\partial T}{\partial y} = 0$$

(b) When the flow is from the right to left,

$$x = L/D \text{ (right inlet)} \quad u = u_{\text{max-y}}(y)\sin(\omega t),$$

$$v = w = T = 0$$

$$x = 0 \text{ (left outlet)} \quad p = \frac{\partial u}{\partial x} = \frac{\partial v}{\partial x} = \frac{\partial w}{\partial x} = \frac{\partial T}{\partial x} = 0$$

$$y = 0, 1 \quad u = v = w = 0, \quad \frac{\partial T}{\partial y} = 0$$

(c) At the heater:

$$T = T_s \quad \text{(constant)}$$

where $u_{\text{max-y}}(y)$ is the maximum (referred to time) inlet velocity profile. For a uniform inlet profile, $u_{\text{max-y}}(y) = u_{\text{max-m}}$. Also, it is important to note that heat transfer enhancement at the heater due to the oscillatory flow shows up in the temperature of the exiting air from the channel at the two ends.

4. Simulation cases and numerical computations

As already pointed out, several sets of data of [2] will be utilized to compare with results of the present study. However, because of some uncertainties in the experimental data, as will be described later, comparisons are not to be based on predicting independently the experimental data by the present numerical results, but only to provide a basis to ascertain that the computed results do agree with the trends of the data. If this can be established, then the physical discussions that follow can be made with some degree of confidence. Four experimental cases with relatively low L/D have been simulated, covering a large range of oscillatory-flow Reynolds numbers, as given in Table 1. They are referred to as Cases 1, 2, 3, and 4, according to decreasing heights of the channel. Unfortunately, the measured maximum centerline velocities $u_{\text{mea-c}}$, in Table 1, did not show consistent relation with parameters α and β. It is suspected that the most probable reason is that air leakages occurred in the test loop outside the test section. The actual air volume through the test section and therefore the tidal displacements and the maximum velocities are all less than the calculated data based on no-leakage conditions. Since the frequency of the oscillatory-flow driver, the test-loop geometries, and the axial velocities at the channel center can all be accurately measured, the unmeasured velocity profiles at the channel inlet must be modified and corrected for the purpose of carrying out the numerical simulations. The flow rates obtained by integrating the experimental velocity data are used as that at the inlet because of conditions of an incompressible fluid. The inlet velocity profiles are also needed in the simu-

Table 1
Numerical simulation cases

Case No.	Case 1	Case 2	Case 3	Case 4
D (cm)	7.595	5.702	3.810	1.905
α	13.08	11.34	7.58	4.64
β	603	1012	1515	567
Re_ω	7887	11,476	11,484	25,831
$u_{\text{mea-c}}$ (m/s)	1.60	2.10	2.50	9.50
Ri	0.08	0.03	0.01	0.0002
L/D	6.19	8.24	12.34	24.67
W/D	2.01	2.67	4.00	8.00
f (H_z)	0.3	0.4	0.4	0.6
Δ_x (m)	1.75	2.54	3.80	11.40

lations. Two such profiles have been tried. One is the simple uniform profile based on the corrected flow rate, and the second, known as the revised inlet condition, is based on the measured maximum (referred to time) velocity profile located at the middle of the channel (referred to the x-direction). The premise here is that in view of the fact that the channel is quite short, the velocity profiles inside the channel are not expected to be sensitive to the axial channel positions. Even though other possibilities are also available, these two trial profiles are considered to be adequate for the intended purpose of this study. All numerical results obtained to compare with the experimental data are based on three-dimensional computations which also include the buoyancy effects, despite the fact that the Richardson numbers are small for all the cases simulated, as shown in Table 1. Some additional two-dimensional simulation cases have also been calculated so that the three-dimensional effects can be determined.

Insofar as the numerical computations are concerned, accuracy, numerical stability, computational

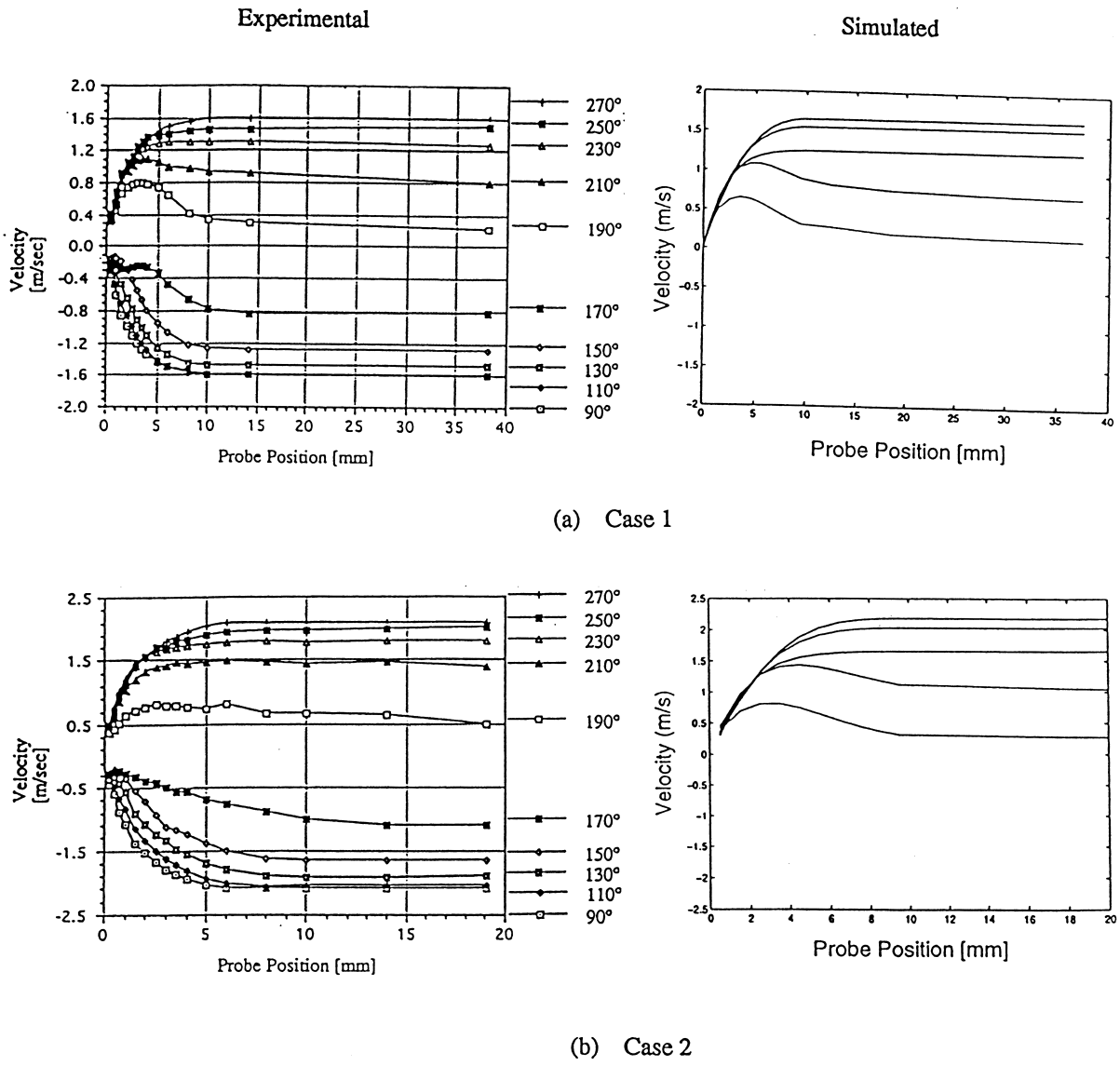

Fig. 2. Comparison of mean velocity profiles based on the revised inlet condition.

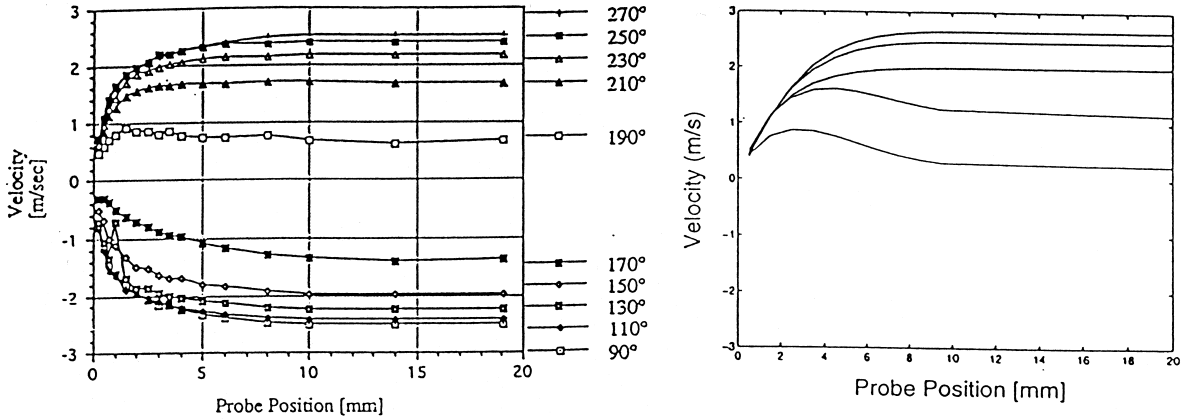

(c) Case 3

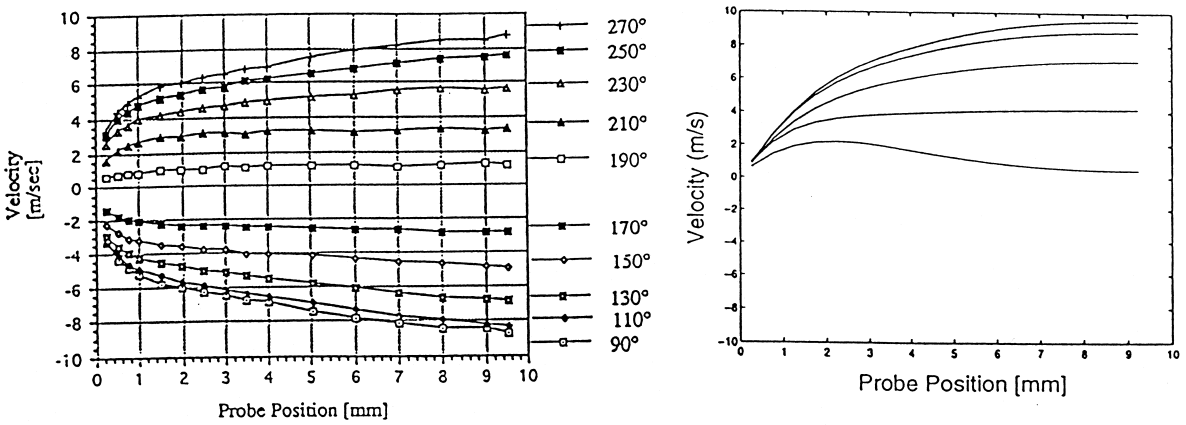

(d) Case 4

Fig. 2 (*continued*)

efficiency, and numerical consistency are often the basis of choosing a numerical method of solving the governing equations in a given problem. The control-volume finite-difference method, which largely satisfies these criteria, has been chosen in the present case. In particular, the QUICK [16] scheme for differencing the advection and convection terms provides less numerical error than many of other simulation models. The computational code has been extensively tested successfully in three-dimensional, two-dimensional, and time dependent cases with known accurate results, along with grid-refinement studies including the Richardson extrapolation, all based on uniform cell structures [17]. For three-dimensional calculations, a satisfactory grid of $54 \times 77 \times 22$ cells has been used, while a grid of 54×77 cells is used for the two-dimensional cases.

5. Numerical simulation results

Of the two trial velocity profiles, the one based on the revised inlet condition, has been found to be consistently better in the comparisons with the experimental measurements, even though the one based on the uniform profiles requires much less computational effort and still give reasonable results. The comparisons of the mean velocity profiles of the four simulation cases at the middle section of the channel as a function of the distance from the bottom wall are shown in Fig. 2. The angles referred to in the experimental data on the left are the crank positions of the oscillatory-flow driver, covering an entire cycle. However, only those from 180° to 360° are shown in the simulated results because of symmetry.

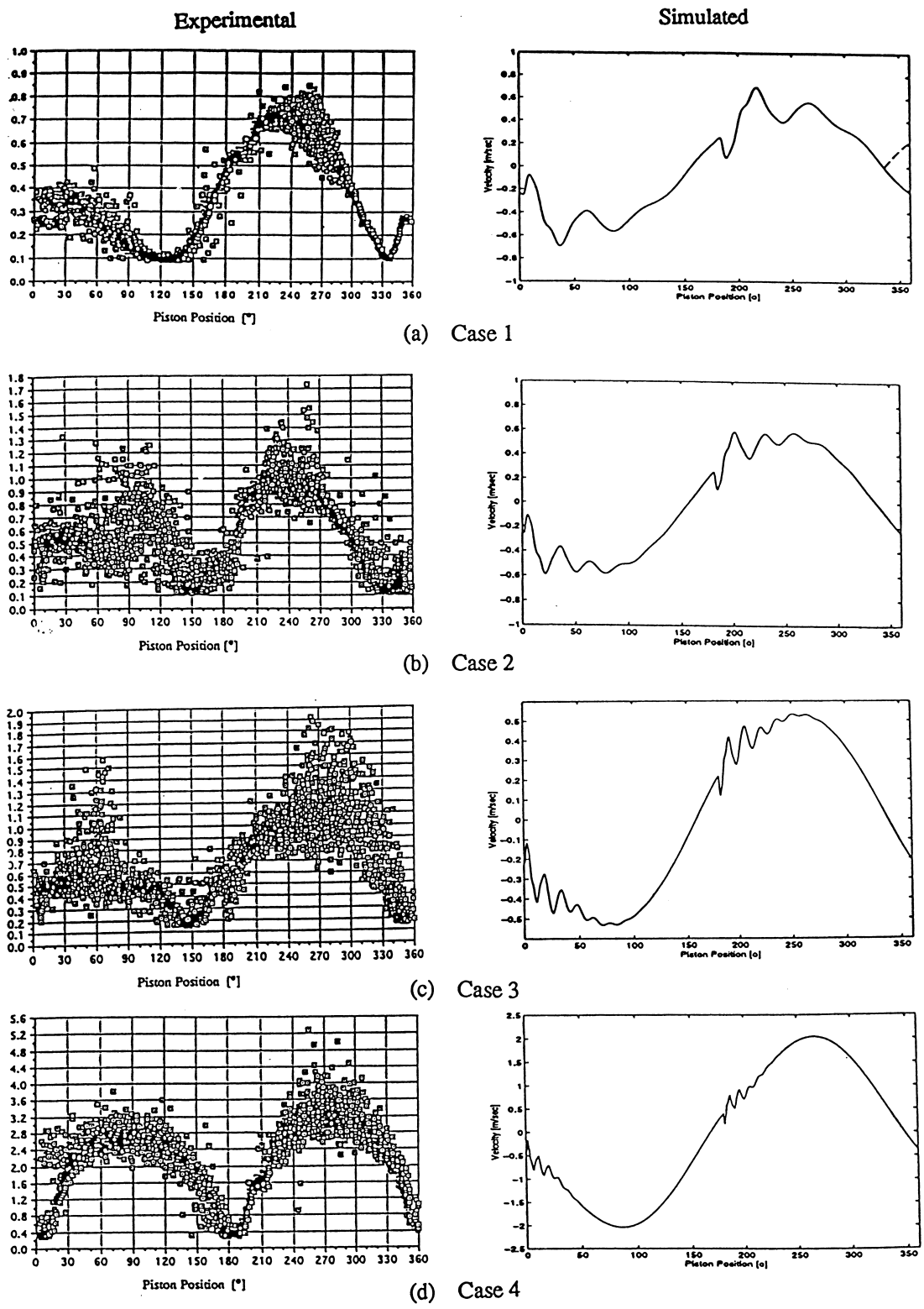

Fig. 3. Comparison of velocity time series based on the revised inlet condition at $y = 0.0013$.

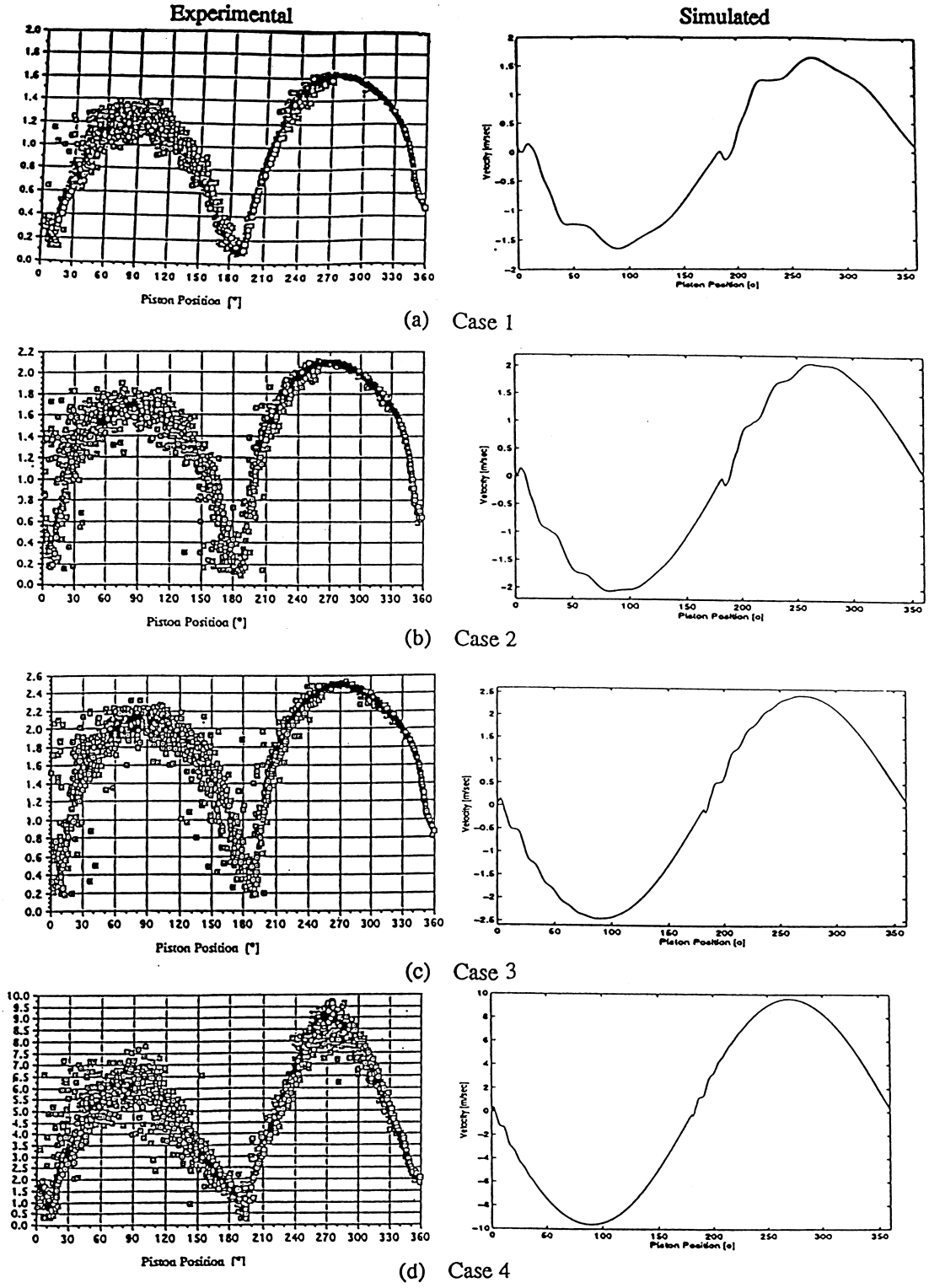

Fig. 4. Comparison of velocity time series based on the revised inlet condition at $y = 0.5$.

It is clearly seen that the simulated results are reasonable both in the profile shapes and local velocities throughout the relatively large range of oscillatory Reynolds numbers. In Cases 1, 2, and 3, the results show that the mean flows are boundary-layer like along the entire channel length. On the other hand, Case 4 suggests more of a fully-developed situation corresponding to cases of large L/D ratios, which is somewhat expected because of the small channel height. More detailed comparisons of the flow field can also be obtained by examining the local axial velocity time series, as shown in Fig. 3 at a distance of $y = 0.013$, close to the bottom wall, and in Fig. 4 at the half height of the channel ($y = 0.5$). The experimental data shown in Figs. 3 and 4 unfortunately are not plotted in the proper time series for a given cycle, but composite plots over many cycles that include local uncertainty variations. Also, the data for the front half of the cycle shown are not accurate because of probe interference [2]. However, the existence of intracycle oscillations in these cases is indisputable, since similar intracycle oscillations have been found experimentally by many other researchers under similar oscillatory-flow situations [11–14]. In fact, the experimental time series for these cases of horizontal velocities were available when the experiments were being carried out, and unfortunately they are no longer available at the present time [17]. Another interesting

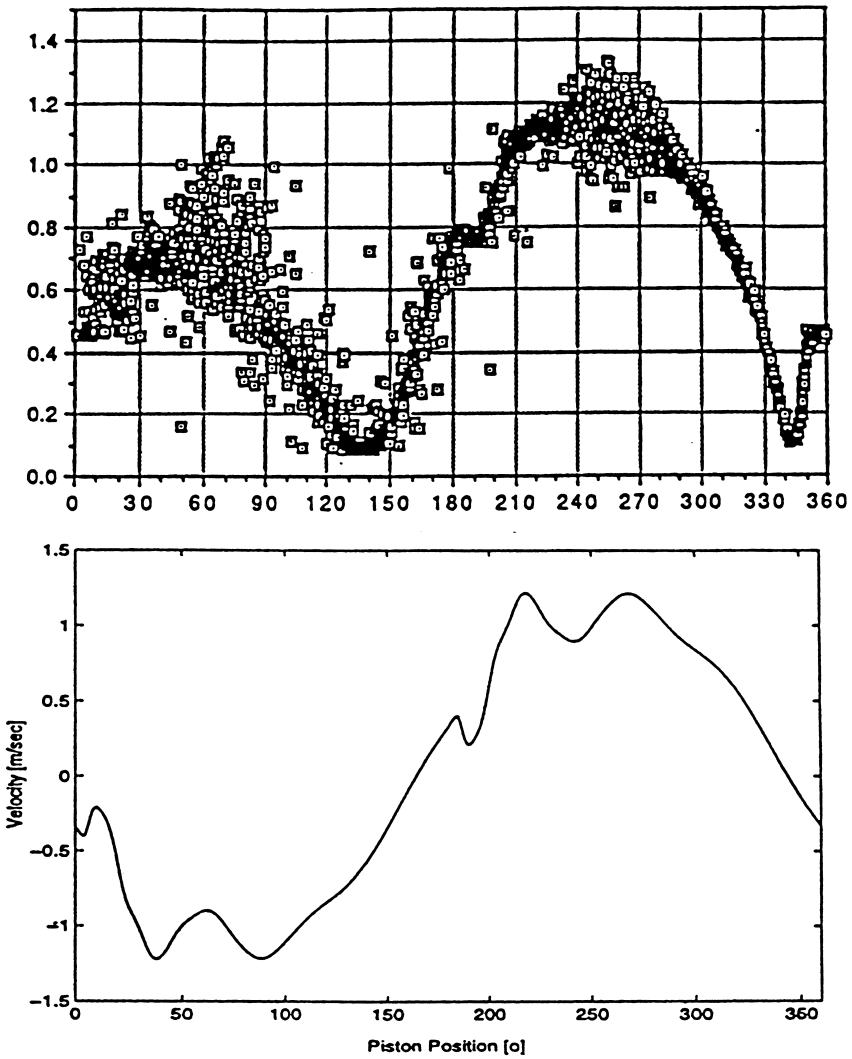

Fig. 5. The velocity jump after 180° at $y = 0.032$ for Case 1.

point is that such intracycle have been calculated from completely laminar equations, and there is no reason to expect that they are in any way related to turbulence.

For the largest height case, Case 1, the numerical results and experimental data agree well with each other (Fig. 3a). The maximum values are almost the same at both height levels. The phase lead is about 30° at $y = 0.013$. It is shown by the velocity time series between 330° and 360°, numerically and experimentally. Here again, the probe's blindness "bends" the plot in the experiment. The dashed line in the simulation is plotted to compare with the experiment. Only a few degrees of phase lag happen at $y = 0.5$ (Fig. 4). Both the experiment and simulation show that intracycle oscillations occur at $y = 0.013$ during both the accelerating and decelerating phases of the cycle. On the other hand, intracycle oscillations only occur during the accelerating phase at $y = 0.5$. This somewhat contradicts with what has been observed by several past investigators, while it is also alluded to by Hino et al. [12], Ohmi et al. [13], and von Kerczek and Davis [18]. This confusion arises because of the fact that the underlying mechanisms have so far not been completely characterized. In accordance with the present results, it can be argued that the intracycle oscillations occurring in the accelerating phase are the characteristics of the specific boundary conditions encountered in short channels.

As the channel height decreases in Cases 2 to 4, the comparisons shown in Figs. 3 and 4 are still reasonably good. The piston positions where the maximum velocities occur are in good agreement at both height levels. The intracycle oscillations at $y = 0.5$ still occur mostly in the accelerating phase. However, it can also be observed that the simulated maximum velocities at $y = 0.013$ are all smaller than those in the experiments, suggesting that as the channel height decreases, near-wall oscillations tend to occur only in the accelerating phase and have small amplitudes. The velocity variations at half height of the channel decrease as well in the simulations. This tendency is primarily due to the increased L/D, as the end effects are reduced.

It is interesting to note that there is a jump just after 180°. The comparison between the simulation and experiment at $y = 0.032$ in Case 1 shows the jump more clearly (Fig. 5). It is caused by the pressure discontinuity when the flow reverses and the exhaust door opens suddenly. Based on the characteristic pressure $\rho u^2_{\text{max-m}}$, the dimensionless pressure time series at $y = 0.032$ at the right end of the channel is plotted to show the sudden changes, as shown in Fig. 6.

When the piston position is between 180° and 360°, the flow is from right to left, the pressure at the right end of the channel varies with time. At 360°, the exhaust door at the right end suddenly opens to the ambient, where the pressure p is set to be zero. This is the reason for the pressure discontinuity and the velocity oscillations during the acceleration phases.

Additional simulations for the same four cases have been carried out with the corresponding two-dimensional computations. It suffices to indicate that with

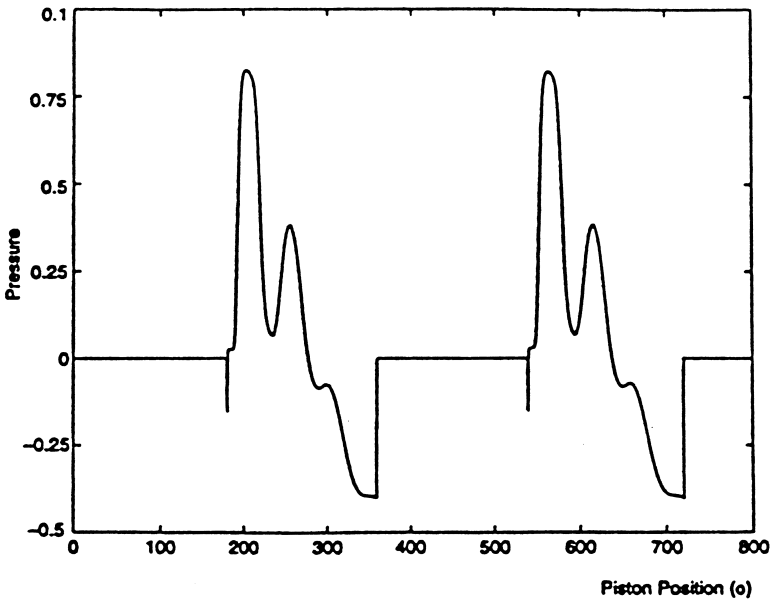

Fig. 6. The pressure discontinuity at $y = 0.032$ for Case 1.

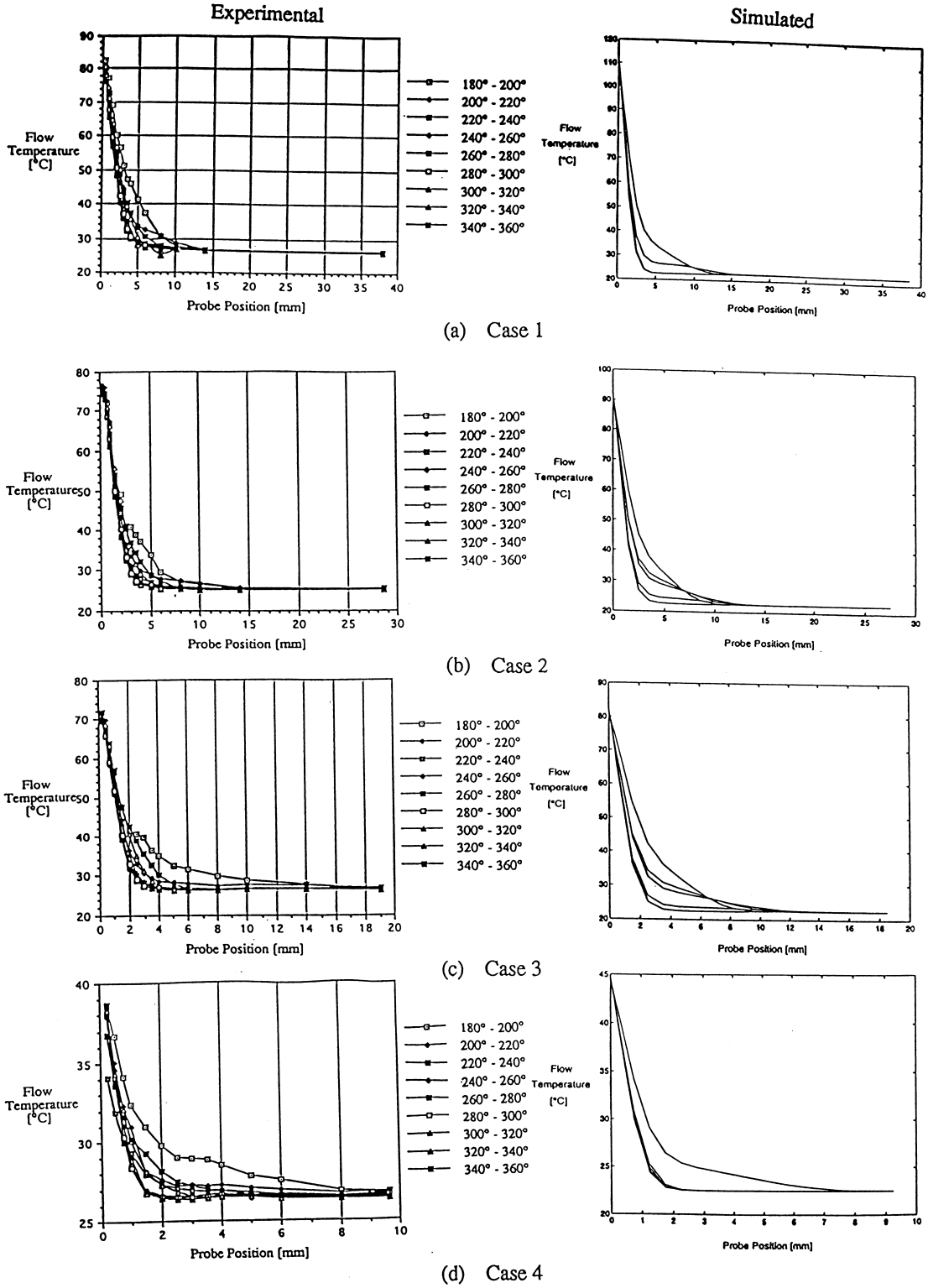

Fig. 7. Comparison of mean temperature profiles.

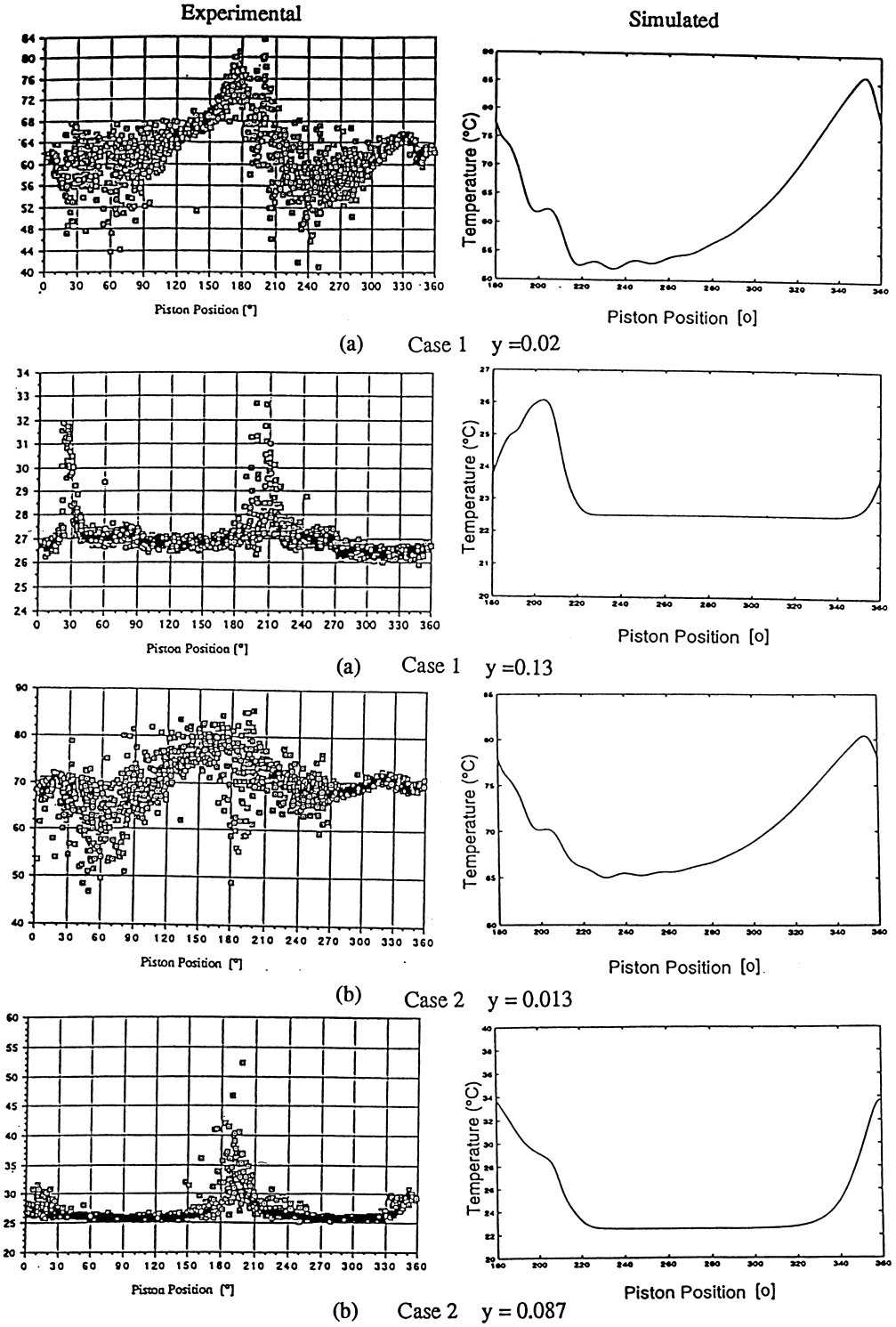

Fig. 8. Comparison of local temperature time series.

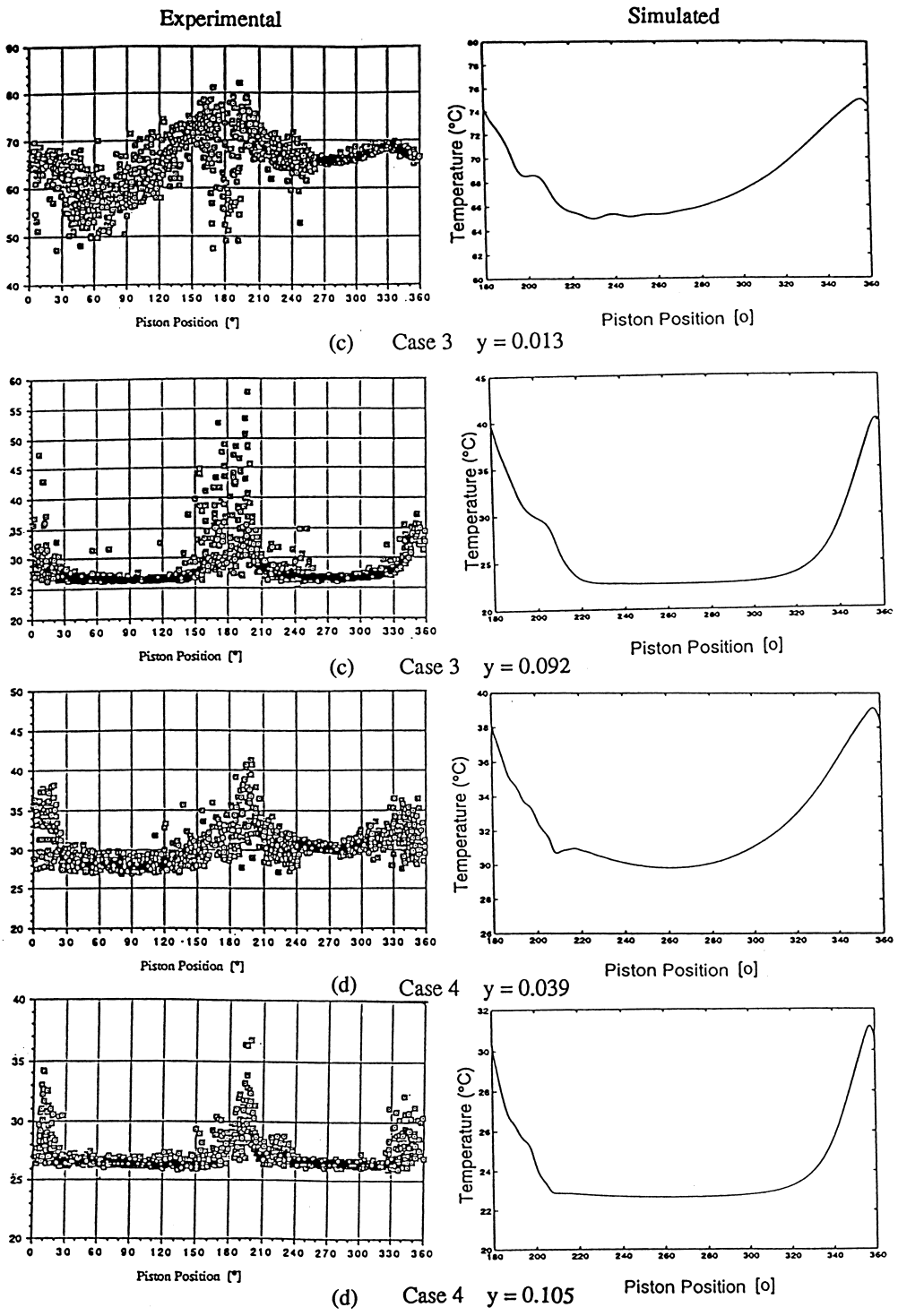

Fig. 8 (*continued*)

the third dimension included in the three-dimensional calculations, the increased mobility of flow in this added dimension gives larger intracycle velocity oscillations and lead actually to better agreement with the experimental data in all cases.

Once the simulated velocity field is known for all four cases, the corresponding temperature field can then be calculated from the energy equation with the boundary conditions given previously. It is however, important to be reminded that a conjugate model has also been used to treat the heater at the center of the channel floor. The comparisons between the experimental data and the simulated results for all the simulated cases in terms of the mean temperature profiles and the local temperature series are shown in Figs. 7 and 8, respectively. In the time series plots, only the back halves of the cycles are given, since the experimental data for the front halves again are not accurate because of probe interference. The latter results are also shown at two height levels, both of which are fairly close to the wall.

For all cases shown, it is seen that the simulated temperature fields indicate the presence of thermal boundary layers and that the boundary-layer behaviors agree well with that of the experiments. For Case 1, two levels at $y = 0.02$ and 0.13 are chosen (Fig. 8a). Reasonably good temperature level comparisons can be observed over the range of the back half of the cycle. At the lower level, there is a shift in the experimental data in the last 30° of the cycle. The reason is the same as that in the flow field, i.e. the way in which the probe can only respond to flow in one direction once the probe is placed in the flow. There the maximum temperature occurs at 352°, while at $y = 0.13$, it occurs at 382°, a phase shift of about 30°. Level pairs of $y = 0.013$, 0.087; $y = 0.013$, 0.092; and $y = 0.039$, 0.105 have been chosen for plotting purposes for Cases 2, 3, and 4 in Fig. 8b–d, respectively, where the simulation gives somewhat lower temperatures between 220° and 320°. One probable reason is that the end effects due to pressure discontinuity at the outlet could not be accurately modeled. Despite some minor discrepancies, the laminar-flow simulations of both the velocity and temperature fields over a wide range of the oscillatory-flow Reynolds number compare well with the corresponding experimental data. Even though turbulence could occur in other zero-mean oscillatory-flow parameter space, it is certainly true that no turbulence could occur in the short-channel phenomena studied here, and the heat transfer enhancement is primarily due to the specific end effects which generate intracycle oscillations, particularly in the accelerating phase of the cycle, and thus promote increased heat transfer by better mixing.

6. Conclusions

The present study deals with the three-dimensional numerical simulations of zero-mean oscillatory flows in short channels with the purpose of determining the underlying mechanism for the observed heat transfer enhancement. Four simulation cases with a discrete heater at the mid-channel floor and covering a wide range of oscillatory-flow Reynolds numbers at several L/D ratios have been treated and the results compared with the corresponding experimental data. The following conclusions can be made:

1. Despite some uncertainties regarding the experimental data, the simulation results compare well with the data for both the velocity and temperature fields, including the time series within the oscillation cycle.
2. Intracycle oscillations have also been found in the simulations. However, such oscillations occur during the accelerating phase of the base-flow cycle, the same as in the experimental data. It is argued that such behavior is the direct result of sudden pressure changes at the channel outlets inherent in the experimental data, and that such end conditions affect directly the flow and heat transfer behaviors inside the channel.
3. Such intracycle oscillations promote fluid mixing and thus lead to enhanced heat transfer. However, since the simulations are based entirely on laminar equations and the results compare well with the experimental data, it is now certain that flows covered by the range of oscillatory-flow Reynolds number and L/D ratio used in the present simulations are not turbulent flow, nor are they related to strong nonlinear instabilities associated with long channels or ducts.

Acknowledgements

This study is one of a continuing series of studies originally funded by IBM, Endicott, NY. The senior author also received a research assistantship from the Tyler Refrigeration Corporation, Niles, MI during the course of this study. These financial supports are gratefully acknowledged.

References

[1] W.L. Cooper, V.W. Nee, K.T. Yang, Fluid mechanics of oscillatory and modulated flows and associated applications in heat and mass transfer — a review, Journal of Energy, Heat and Mass Transfer 15 (1993) 1–19.
[2] W.L. Cooper, V.W. Nee, K.T. Yang, An experimental

investigation of convective heat transfer from the heated floor of a rectangular duct to a low frequency, large tidal displacement oscillatory flow, International Journal of Heat and Mass Transfer 37 (1994) 581–592.

[3] T. Zhao, P. Cheng, Oscillatory heat transfer in a pipe subjected to a periodically reversing flow, International Journal of Heat and Mass Transfer 38 (1995) 3011–3022.

[4] S.G. Qiu, T.W. Simon, Measurements of heat transfer and fluid mechanics within an oscillatory flow in a pipe, in: Fundamentals of Heat Transfer in Forced Convection, HTD 285, ASME, New York, 1994, pp. 1–7.

[5] T.E. Walsh, K.T. Yang, V.W. Nee, Q.D. Liao, Forced convection cooling in microelectronic cabinets via oscillatory flow techniques, in: Exp. of Heat Transfer, Fluid Mech. and Thermo, Elsevier, Amsterdam, 1993, pp. 641–648.

[6] Q.D. Liao, K.T. Yang, V.W. Nee, Enhanced microprocessor chip cooling by channeled zero-mean oscillatory air flow, in: Advances in Electronic Packaging, vol. 2, ASME, New York, 1995, pp. 789–794.

[7] J.G. Zhang, U.H. Kurzweg, Numerical simulation of time-dependent heat transfer in oscillatory pipe flow, Journal of Thermophysics and Heat Transfer 5 (1991) 401–406.

[8] T. Zhao, P. Cheng, Experimental studies of a cyclically turbulent oscillatory flow in a pipe, International Journal of Heat and Fluid Flow 16 (1995) 90–97.

[9] H.J. Huang, K.T. Yang, V.W. Nee, Simulation of nonlinear oscillations of laminar forced convection cooling with zero-mean oscillatory flow in an open channel, in: Chaos in Heat Transfer and Fluid Dynamics, HTD 298, ASME, New York, 1994, pp. 19–25.

[10] H.J. Huang, K.T. Yang, V.W. Nee, Simulation of forced air cooling of a discrete heat source in an open enclosure by zero-mean oscillatory flow, in: Advances in Electronic Packaging, vol. 2, ASME, New York, 1995, pp. 795–800.

[11] S.I. Sergeev, Fluid oscillations in pipes at moderate Reynolds numbers, Fluid Dynamics 1 (1966) 121–122.

[12] M. Hino, M. Sawamoto, S. Takasu, Experiments on transition to turbulence in an oscillating pipe flow, Journal of Fluid Mechanics 75 (1976) 193–207.

[13] M. Ohmi, M. Iguchi, I. Urahata, Flow patterns and frictional losses in an oscillating pipe flow, Bulletin of JSME 25 (1982) 536–543.

[14] P. Merkli, H. Thomann, Transition to turbulence in oscillating pipe flow, Journal of Fluid Mechanics 68 (1975) 567–575.

[15] U.H. Kurzweg, E.R. Lindgren, B. Lothrop, onset of turbulence in oscillating flow at low Womersley number, Physics of Fluids A 1 (12) (1989) 1972–1975.

[16] B.P. Leonard, Elliptic systems: finite-difference method IV, in: W.J. Minkowycz, E.M. Sparrow, G.E. Schneider, R.H. Pletcher (Eds.), Handbook of Heat Transfer, Wiley, New York, 1998, pp. 9.347–9.378.

[17] P. Li, Hydrodynamic stability and heat transfer in zero-mean oscillatory flows in short and long channels, Ph.D. Thesis, University of Notre Dame, Notre Dame, IN, 1997.

[18] C. von Kerczek, S.H. Davis, Linear stability theory of oscillatory stokes layers, Journal of Fluid Mechanics 62 (1974).